AD-A188 228 AN ANALYSIS OF WHISTLER-MODE RADIATION FROM THE SPACELAB-2 ELECTRON BEAM..(U) IOWA UNIV IOWA CITY DEPT OF PHYSICS AND ASTRONOMY W M FARRELL ET AL. 07 AUG 87 1/1

UNCLASSIFIED U. OF IOWA-87-19-REV N00014-85-K-0404 F/G 20/14 NL

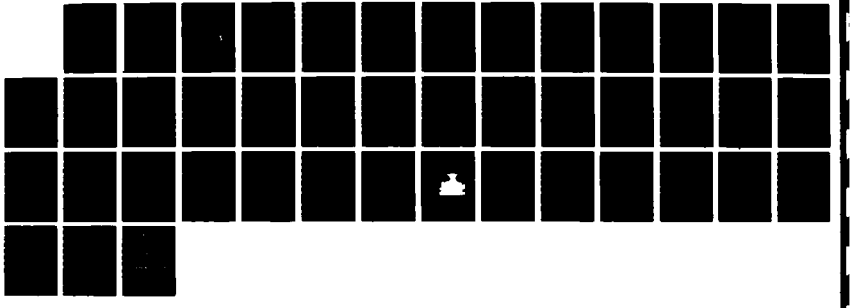

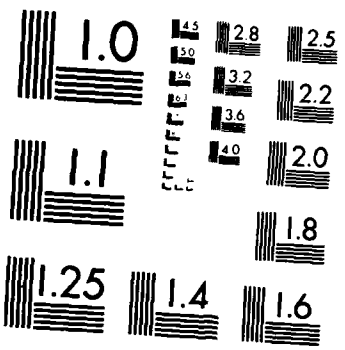

AN ANALYSIS OF WHISTLER-MODE RADIATION FROM THE SPACELAB-2 ELECTRON BEAM

by

W. M. Farrell[1], D. A. Gurnett[1],
P. M. Banks[2], R. I. Bush[2] and W. J. Raitt[3]

Department of Physics and Astronomy
THE UNIVERSITY OF IOWA
Iowa City, Iowa 52242

(1)

AN ANALYSIS OF WHISTLER-MODE RADIATION FROM THE SPACELAB-2 ELECTRON BEAM

by

W. M. Farrell[1], D. A. Gurnett[1],
P. M. Banks[2], R. I. Bush[2] and W. J. Raitt[3]

January 1987

21- Revised June 1987

Submitted for publication to J. Geophys. Res.

[1]Dept. of Physics and Astronomy, The University of Iowa, Iowa City, Iowa 52242

[2]STAR Laboratory, Stanford University, Stanford, California 94305

[3]Center for Atmospheric and Space Sciences, Utah State University, Logan, UT 84322

UNCLASSIFIED

SECURITY CLASSIFICATION OF THIS PAGE (When Data Entered)

A188 228

REPORT DOCUMENTATION PAGE

READ INSTRUCTIONS BEFORE COMPLETING FORM

1. REPORT NUMBER: U. of Iowa 87-19 -REV	2. GOVT ACCESSION NO.
3. RECIPIENT'S CATALOG NUMBER	
4. TITLE (and Subtitle): AN ANALYSIS OF WHISTLER-MODE RADIATION FROM THE SPACELAB-2 ELECTRON BEAM	5. TYPE OF REPORT & PERIOD COVERED: Progress June 1987
6. PERFORMING ORG. REPORT NUMBER	
7. AUTHOR(s): W. M. Farrell, D. A. Gurnett, P. M. Banks, R. I. Bush, and W. J. Raitt	8. CONTRACT OR GRANT NUMBER(s): N00014-85-K-0404
9. PERFORMING ORGANIZATION NAME AND ADDRESS: Department of Physics and Astronomy, The University of Iowa, Iowa City, IA 52242	10. PROGRAM ELEMENT, PROJECT, TASK AREA & WORK UNIT NUMBERS
11. CONTROLLING OFFICE NAME AND ADDRESS: Office of Naval Research, Electronics Program Office, Arlington, VA 22217	12. REPORT DATE: 7 August 1987
	13. NUMBER OF PAGES: 40
14. MONITORING AGENCY NAME & ADDRESS (if different from Controlling Office)	15. SECURITY CLASS. (of this report): UNCLASSIFIED
	15a. DECLASSIFICATION/DOWNGRADING SCHEDULE

16. DISTRIBUTION STATEMENT (of this Report)

Approved for public release; distribution is unlimited

17. DISTRIBUTION STATEMENT (of the abstract entered in Block 20, if different from Report)

18. SUPPLEMENTARY NOTES

To be published in J. Geophys. Res.

19. KEY WORDS (Continue on reverse side if necessary and identify by block number)

Electron Beam
Whistler-mode emissions
Beam Plasma Interactions

20. ABSTRACT (Continue on reverse side if necessary and identify by block number)

(See page Following)

DD FORM 1 JAN 73 1473 EDITION OF 1 NOV 65 IS OBSOLETE
S/N 0102-LF-014-6601

UNCLASSIFIED

SECURITY CLASSIFICATION OF THIS PAGE (When Data Entered)

ABSTRACT

During the shuttle's Spacelab-2 mission, the ~~University of~~ Iowa's Plasma Diagnostics Package (PDP) was released from the shuttle to freefly. At times during this freeflight when the PDP was magnetically connected to the shuttle, ~~Stanford's~~ Fast Pulsed Electron Generator (FPEG), located in the shuttle cargo bay, ejected a 1 keV - 50 mA electron beam. The plasma wave instrument on board the PDP detected intense whistler-mode radiation during these beam ejections. This paper presents a study of a whistler-mode emission detected during one particular continuous electron beam firing. Calculations indicate that the beam radiated approximately 1.6 mW in the whistler mode as the beam traversed the 200 meters from the shuttle to the PDP. The emissivity also decreased by about a factor of 10 over this same distance. The measured wave powers are 10^7 greater than wave powers expected from incoherent Cerenkov radiation, verifying that the radiation is generated by a coherent process. Estimates of the emissivity based on measured electric field intensities in the beam indicate that the whistler-mode noise is produced by radiation from electron bunches created by an electrostatic beam-plasma instability.

INTRODUCTION

In this paper we describe an electron beam experiment performed on the Spacelab-2 mission. The Spacelab-2 flight, which was launched on July 29, 1985, included an electron accelerator called the Fast Pulsed Electron Generator (FPEG) from Stanford University, and a spacecraft called the Plasma Diagnostics Package (PDP) from the University of Iowa. During a 6-hour period on August 1, 1986, the PDP was released from the shuttle to investigate plasma effects in the vicinity of the shuttle. During the PDP free flight, the shuttle was maneuvered so that the PDP passed near magnetic field lines connected to the shuttle. Four such magnetic conjunctions were achieved. During one of these magnetic conjunctions a 1 keV - 50 mA electron beam was continuously ejected from the shuttle so that radiation effects could be monitored as the PDP passed near the magnetic field line carrying the beam. Figure 1 shows a frequency vs. time spectrogram from the PDP plasma wave instrument during this electron beam event. The funnel-shaped signal extending from the electron cyclotron frequency, f_c, down to approximately 30 kHz is whistler-mode radiation from the electron beam. This whistler-mode radiation was first described by Gurnett et al. [1986]. Our objectives in this paper will be to determine the total radiated power from the beam and compare it with the power predicted by various whistler-mode radiation mechanisms.

Whistler-mode emissions are known to be produced by both artificial and natural electron beams. Some of the early observations of emissions from artificial electron beams were made in the early seventies by the University of Minnesota group using the Echo rocket experiments [Cartwright and Kellogg, 1974; Kellogg et al., 1976; Monson et al., 1976; Winckler, 1980]. Observations of beam-generated emissions were also made on the joint Franco-Soviet ARAKS beam experiments [Dechambre et al., 1980]. The first space shuttle electron beam experiment was performed in March, 1982, as part of the STS-3 mission. On this flight, the PDP was carried on the shuttle remote manipulator arm and the FPEG was used to produce an artificial electron beam. During electron gun firings, a possible whistler-mode signal was detected from the electron beam [Shawhan et al., 1984]. In December of 1983, the Phenomenon Induced by Charged Particle Beams (PICPAB) experiment was carried as part of the Spacelab-1 mission. The PICPAB experiment was specifically designed to investigate radiation from electron beams injected in the ionosphere. Like the other previous experiments, whistler-mode signals were again detected when the electron gun was fired [Beghin et al., 1984].

Whistler-mode radiation is also produced in the auroral zone in association with the field-aligned electron beams that are responsible for the aurora [Gurnett, 1966]. This radiation is usually called auroral hiss. Both upward and downward propagating auroral hiss has been observed [Mosier and Gurnett, 1969]. The downward propagating auroral hiss is associated with downward moving electron beams with

characteristic energies of a few hundred eV [Gurnett, 1966; Hartz, 1969; Gurnett and Frank, 1972; Laaspere and Hoffman, 1976]. The upward propagating auroral hiss often has a V-shaped spectrum called a "saucer" [Smith, 1969; Mosier and Gurnett, 1969; James, 1976] or a "funnel" [Gurnett et al., 1983]. Upward propagating auroral hiss has been observed in association with upward moving field-aligned electron beams [Lin et al., 1984]. The characteristic frequency-time shape of the "saucer" or "funnel" is a propagation effect that occurs for whistler-mode waves propagating near the resonance cone. Gurnett et al. [1986], in their initial analysis of the Spacelab-2 results, showed that a similar wave propagation effect was observed for the whistler-mode signals generated by the SL-2 electron beam.

ELECTRIC FIELD POLARIZATION

To confirm that the radiation from the Spacelab 2 electron beam is propagating in the whistler mode, we compare the electric field polarization with the polarization expected for the whistler mode. The whistler mode has a polarization that depends on the wave frequency, f, the wave normal angle, θ, the cyclotron frequency, f_c, and the plasma frequency, f_p. Using cold plasma theory [Stix, 1962], the electric-field and index of refraction vectors can be calculated as a function of f, θ, f_c, and f_p. For the whistler mode the index of refraction varies strongly as a function of the wave normal direction. This variation can be represented by an index of refraction surface, $\overline{n}(\theta)$, which is a surface that is defined by the loci of index of refraction vectors at different wave normal angles. Figure 2 shows the index of refraction surface for the whistler mode. At a limiting wave normal angle, known as the resonance cone angle, θ_{Res}, the index of refraction goes to infinity. The resonance cone angle is given by $\tan^2\theta_{Res} = -P/S$, where $P = 1 - f_p^2/f^2$ and $S = 1 - f_p^2/(f^2 - f_c^2)$. As the wave normal approaches the resonance cone, the electric field $\overline{E}$ becomes linearly polarized with $\overline{E}$ parallel to $\overline{n}$. In this limit the electric field is quasi-electrostatic and the group velocity, $\overline{v}_g$, is perpendicular to $\overline{E}$ $\overline{n}$ (see Figure 2).

In a previous paper [Gurnett et al., 1986], the funnel-shaped frequency versus time pattern of the radiation from the SL-2 electron

beam was explained as a frequency dependent propagation effect for whistler-mode emissions from the electron beam. Figure 3 is a sketch demonstrating how this effect works. Consider, first, a point source of whistler-mode radiation, with the radiation propagating near the resonance cone. As the wave frequency increases, the resonance cone angle decreases and the ray path direction, $\bar{v}_g$, becomes increasingly oblique to the magnetic field, approaching 90° as the frequency approaches the electron cyclotron frequency. Typical ray paths for a whistler-mode emission propagating near the resonance cone are shown in the figure. As a spacecraft approaches the source, emissions near the gyrofrequency are detected first, since their ray paths are almost perpendicular to the beam. Lower and lower frequencies are then detected as the distance between the spacecraft and source decreases. This frequency dependent propagation effect creates a funnel-shaped emission pattern on a frequency versus time spectrogram. By comparing a modeled emission pattern using cold plasma theory to the funnel-shaped pattern shown in Figure 1, Gurnett et al. [1986] have confirmed that the whistler-mode emission from the SL-2 electron beam is propagating upward from the shuttle near the resonance cone. The distinct funnel boundary is defined by the waves that propagate directly from the beam origin, the shuttle. The funnel on the spectrogram appears filled-in since the radiation is being emitted by a line source extending upward from the shuttle rather than a point source. Since the waves are upward propagating, $\bar{k}\cdot\bar{v}_b > 0$, where $\bar{v}_b$ is the beam velocity vector.

In order to provide further confirmation that the radiation from the SL-2 electron beam is propagating near the resonance cone, an

additional test was performed. This test compares model electric-field directions in the PDP spin plane to their actual directions as measured by the PDP plasma wave instrument. To perform this test a computer program was developed that calculates the angle, ϕ, between the projection of a model electric field onto the spin plane and a fixed reference direction. The fix reference direction selected was the spin plane projection of the spacecraft-sun vector. To compute ϕ, the group velocity was assumed to be directed from a point on the beam toward the PDP with the electric field vector, $\overline{E}$, at an angle θ_{Res} relative to the beam. This field geometry is the expected configuration for an upward propagating whistler-mode wave near the resonance cone. Figure 4 shows the corresponding geometry of $\overline{E}$, $\overline{v}_g$ and $\overline{k}$.

The electric-field directions in the spin plane calculated using the model described above are compared to the measured electric-field directions found from spin modulation maximums in the receiver data. The spin modulation maximums occur when the PDP electric antennas are aligned with the measured electric field in the spin plane, thus allowing a direct determination of this measured electric field direction. Figure 5 shows the results of this comparison at four frequencies: 562, 311, 178, and 100 kHz. This figure shows the phase angle, ϕ, between the projected electric field and the sun vector as a function of time. The dots represent the modeled electric-field directions computed assuming a resonance cone propagation scheme while the X's represent the measured electric-field directions. The close agreement between the computed and measured electric field directions

provides strong confirmation that the waves are propagating near the resonance cone and in the beam direction (i.e., $\overline{k} \cdot \overline{v}_b > 0$), as indicated in Figure 4.

EMITTED POWER

In this section we estimate the total power radiated from the beam in the whistler mode. By comparing the radiated power to the total power in the beam, the efficiency of the wave-beam interaction can be estimated and compared with various generation mechanisms. The power emitted from the beam in the whistler mode can be estimated by integrating the Poynting flux over a surface surrounding the beam. An inherent difficulty with this calculation is the determination of the phase and magnitude of the electric and magnetic fields in the Poynting flux, $\overline{S} = \overline{E} \times \overline{H}$. Since three axis measurements are not available and since phase measurements were not made the Poynting vector cannot be determined directly. Computing the Poynting flux from the electric field alone is complicated by the fact that near the resonance cone the whistler mode is quasi-electrostatic and the ratio of the electromagnetic to electrostatic components is an exceedingly sensitive function of the wave normal angle. To compute the wave normal angle we assume that the radiation is produced by the Landau resonance, i.e., $\omega/k_{\parallel} = v_b$. Since the beam velocity is known, this condition gives a well-defined value for the wave normal direction. The fact that the radiation is propagating in the same direction as the beam ($\overline{k} \cdot \overline{v}_b > 0$) provides a strong indication that the Landau resonance is involved. For example, the $s = -1$ cyclotron resonance

produces radiation propagating in the opposite direction of the beam. Also, as will be discussed later, the Landau resonance gives the best agreement with the measured electric to magnetic field ratios.

To carry out the Poynting vector calculation we note that $\overline{E}$ lies almost entirely in the plane defined by $\overline{n}$ and the geomagnetic field (see Figure 4). The electrostatic and electromagnetic components of $\overline{E}$ are then given by $E_o \cos \Delta\theta$ and $E_o \sin \Delta\theta$, respectively, where $\Delta\theta$ is the angle between $\overline{E}$ and $\overline{n}$, and E_o is amplitude of the total electric field. The angle $\Delta\theta$ is determined by the Landau resonance condition and cold plasma theory. The Landau resonance condition specifies the component of n parallel to the geomagentic field, i.e.,

$$n_{\parallel} = n \cos \theta = c/v_b \quad . \tag{1}$$

where c is the speed of light. For a 1 keV electron beam moving parallel to the magnetic field $n_{\parallel}$ is approximately 15.9. A program was written that solves Equation (1-20) of Stix [1962] for the magnitude and directions of $\overline{n}$ and $\overline{E}$. Equation (1-20) of Stix is

$$\begin{pmatrix} S - n^2\cos^2\theta & -i\,D & n^2\cos\theta\sin\theta \\ i\,D & S - n^2 & 0 \\ n^2\cos\theta\sin\theta & 0 & P - n^2\sin^2\theta \end{pmatrix} \begin{pmatrix} E_x \\ E_y \\ E_z \end{pmatrix} = 0 \tag{3}$$

where

$$S = \frac{1}{2}(R + L) \tag{4}$$

$$D = \frac{1}{2}(R - L) \tag{5}$$

and

$$R = 1 - \sum_k \frac{\omega_{pk}^2}{\omega} \left(\frac{\omega}{\omega + \varepsilon_k \omega_{ck}}\right) \tag{6}$$

$$L = 1 - \sum_k \frac{\omega_{pk}^2}{\omega} \left(\frac{\omega}{\omega - \varepsilon_k \omega_{ck}}\right) \tag{7}$$

$$P = 1 - \sum_k \frac{\omega_{pk}^2}{\omega^2} \quad . \tag{8}$$

The quantities ω_{pk} and ω_{ck} are the plasma and cyclotron frequencies for species k while ε_k is the sign of the charge of species k. Using this program, $\bar{n}$ and $\Delta\theta$ at a particular wave frequency can be calculated consistent with $n_\parallel$. Since $\Delta\theta$ is now determined, the electrostatic and electromagnetic components of $\bar{E}$ can be calculated. The calculated $\Delta\theta$ values are small, typically ranging from .06° to 1.1° from 31.1 kHz to 562 kHz, and indicates that the wave is nearly electrostatic. It is easy to show that the magnitude of the Poynting vector is given by

$$|\bar{S}| = \frac{n E_o^2}{2} \left(\frac{\varepsilon_o}{\mu_o}\right)^{1/2} (A^2 + B^2)^{1/2} \quad , \tag{9}$$

where $A = 1 - \cos^2\Delta\theta$ and $B = \sin\Delta\theta \cos\Delta\theta$. In the derivation of Equation (9) Faraday's Law, $\bar{n} \times \bar{E} = c\bar{B}$, was used to eliminate the magnetic field in the $\bar{E} \times \bar{H}$ term. Consequently, $|\bar{S}|$ is only dependent on $\bar{n}$ and $\bar{E}$ which are well defined quantities. Note, that as θ

approaches the resonance cone angle, n and E become parallel and |S| goes to zero. This behavior near θ_{Res} is similar to an expression derived by Mosier and Gurnett [1971] in their paper addressing Poynting flux measurements of VLF hiss emissions.

Figure 6 shows the PDP trajectory relative to the beam. As can be seen, the PDP trajectory was nearly perpendicular to the beam. At closest approach, it passed within about 3 meters of the beam at a distance of roughly 200 meters from the shuttle. To compute the total radiated power, the Poynting flux is integrated over an imaginary surface perpendicular to the beam that includes the PDP trajectory. Assuming that the sampled intensities along this trajectory are constant around an annular ring of the area, dA, centered on the beam, the radiated power from the beam segment can be obtained by evaluating the integral $P = \int S_{\parallel} 2\pi R dR$, where $S_{\parallel}$ is the field-aligned component of the Poynting vector and R is the perpendicular distance from the beam to the PDP. Note that the evaluation of this integral will yield two values for the radiated power: one value from the inbound pass where the limits of integration extend from $R = \infty$ to $R \cong 0$ and one value from the outbound pass where the limits of the integration now extend from $R \cong 0$ to $R = -\infty$. Figure 7 shows the average power spectral density from these two passes as a function of frequency. The error bars shown in the figure represent the standard deviations of the power values. Note that the power spectral density, dP/df, is on the order of 10^{-9} W/Hz in the frequency range extending from 30 kHz to 1 MHz. The total emitted power in the 200 meter beam segment from the shuttle to the PDP is found to be P = 1.6 mW. Assuming that the power is emitted uniformly

along the beam, the radiated power per unit length, $dP/d\ell$, is approximately 8×10^{-6} W/m. Since the total power of the beam was 50 W, the beam converted approximately 3.2×10^{-5} of its power to whistler-mode radiation in the first 200 meters. If the beam dissipated energy only via the whistler-mode, the beam would only propagate approximately 6000 km before all of the beam energy would be converted to radiation.

The linear emissivity of the whistler-mode radiation, $dP/df d\ell$, from different locations along the beam can also be calculated. To calculate the linear emissivity, a knowledge of a signal's exact source location from the beam is required; however, by using the ray path, the source of the signal at a particular point along the PDP trajectory can be located. The power radiated from an infinitesimal beam radiation source, $d\ell$, is $P = \int S_\perp 2\pi R d\ell$, where $S_\perp$ is the perpendicular component of the Poynting vector measured at the perpendicular distance R from the beam and corresponds to the Poynting flux emitted from a cylinder of radius, R, and length, $d\ell$, surrounding the beam. The linear emissivity from this source, $dP/df d\ell$, is then obtained by using the differential form of the power intergal. The calculated linear emissivity of the whistler-mode waves is shown in Figure 8. Note that the emissivity drops by a factor of ten from 100 to 200 meters along the beam. This decrease in emissivity indicates that the efficiency of whistler-mode generation decreases with increasing distance along the beam and that the generation mechanism is capable of dynamic changes in tens of meters. If the emissivity continues to drop at the rate observed between 100 to 200 meters, the radiation would be undetectable by the PDP at source distances more than about 1 km from the shuttle. This

result may explain why DE-1, which was magnetically connected to the shuttle during a gun firing on the STS-3 mission, did not see beam-generated whistler-mode radiation in the vicinity of the streaming electrons [Inan et al., 1984]. From the SL-2 measurements, it appears that strong whistler-mode emissions are probably generated only in close proximity to the source of the beam.

As mentioned earlier, the electric and magnetic field measurements also provide further evidence that the whistler-mode waves are generated via a Landau resonance process. This argument involves a comparison of computed and measured cB/E ratios. Assuming a specific resonance condition and using the solution of Equations (1-20) of Stix [1962], a unique value for $\overline{n}$ and $\Delta\theta$ can be computed. Faraday's law can then be used to obtain the relationship

$$\overline{n} \times \overline{E} = c\overline{B} \tag{10}$$

where E is in the electric component and B is in the magnetic component of the whistler-mode waves. For the assumed field geometry, Equation (10) can be rewritten as

$$n E_o \text{ Sin } \Delta\theta = cB_o \quad ,$$

or

$$\frac{cB_o}{E_o} = n \text{ Sin } \Delta\theta \quad . \tag{11}$$

Using Equation (11), we can compute n sin $\Delta\theta$ for various resonance conditions and compare this ratio with the measured cB/E ratio. The

spectrum analyzer used with the PDP search coil can only provide measurements up to 178 kHz; therefore, the magnetic to electric field ratio can only be obtained in the 56 kHz, 100 kHz, and 178 kHz frequency channels. Also, the measured values of B at high frequencies using the search coil are highly uncertain, due to inaccuracies in the calibration of the instrument. The preflight calibration was performed by placing a calibration coil in the search coil and surrounding the system in a μ-metal can. A problem arises at high frequencies (>10 kHz), where frequency dependent capacitences and inductances affect the current and the expected value of $\overline{B}$ from the calibration coils. Unfortunately, postflight calibrations under more ideal condition (specifically, without the μ-metal can) have failed to reproduce the preflight calibrations. This suggests that the high frequency gain of the search coil may have shifted during the flight. Our current best estimates are that B (and cB/E) are accurate only to within a factor of 2 - 4 at high frequencies. The range of measured cB/E values lies between 1.3 and 15.3. Assuming a Landau resonance, n sin $\Delta\theta$ is computed to be .54, .52, and .54 for 56 kHz, 100 kHz, and 178 kHz, respectively. Note that these values lie just outside the range of measured cB/E values, and fall in the range when considering the factor of 2 - 4 uncertainty in the calibrations. For an s = +1 cyclotron resonance, however, n sin $\Delta\theta$ is computed to be between .05 to .08 for 56 kHz, 100 kHz, and 178 kHz. These values are about a factor of 20 smaller than the lowest measured cB/E value. Similar computed values are obtained for the s = -1 cyclotron resonance. These comparisons show that the measured cB/E ratio is closest to those expected for a Landau resonance.

INCOHERENT GENERATION MECHANISMS

From the power measurements alone it is not clear whether the beam-generated whistler-mode radiation detected by the PDP during the SL-2 mission results from a coherent or incoherent generation process. A coherent mechanism involves large numbers of particles acting together to generate the emitted waves. The total power from a coherent source goes as N^2, where N is the number of particles in coherence. Common coherent sources are plasma instabilities, lasers and radio antennas. Incoherent mechanisms involve particles that are radiating independently. The power from the individual radiators must be added to get the total power emitted; thus the total power is proportional to N, the number of radiators. A common incoherent source is an incandescent light bulb. This section and the next describe possible incoherent and coherent mechanisms for generating whistler-mode radiation.

One possible incoherent mechanism involves Cerenkov radiation. Cerenkov radiation is caused by charged particles moving with velocities greater than the phase speed of the wave in the medium. The whistler-mode waves from the SL-2 electron beam are propagating near the resonance cone with large index of refractions, typically $n \sim 30$ to 500. The phase speed of the wave is then much less than the speed of the 1 keV electron beam. Since the beam electrons are moving faster than the phase velocity of the whistler mode, Cerenkov radiation should be produced.

The measured whistler-mode power from the beam will now be compared to the calculated power from Cerenkov-radiation, assuming that the beam electrons are incoherent radiators. Our calculations are similar to those performed by Jorgenson [1968] and Taylor and Shawhan [1973], who both calculated the power from this process and compared it to the radiated powers from VLF hiss. Mansfield [1967] derived an equation that gives the power spectral density radiated from a single electron moving through an ambient ionized gas with a speed greater than the wave phase speed. For an incoherent mechanism, the total power radiated from the beam is the power radiated from each electron $(\frac{dP}{df})_e$, added up over all the electrons in a given beam volume, N_V: $(\frac{dP}{df})_{total} = N_V(\frac{dP}{df})_e$. Using Mansfield's formula, the radiated power from each beam electron can be calculated and is shown in Figure 9. In obtaining this result, we assume that the radiation is produced via a Landau resonance. We also assume, for this calculation, that the pitch angle of the electrons is 10°. The actual pitch angles varied from 0° to 20°; however, the results are relatively insensitive to pitch angles in this range. From Figure 9 it can be seen that the most intense radiation occurs between the electron cyclotron frequency and the lower hybrid frequency, f_{LHR}. Outside this range the power drops by a factor of 10^4. Note that this frequency range corresponds rather well to the frequency range of the radiation observed by the PDP. Multiplying the power from each electron by the number of electrons in the first 200 meter segment of the beam (3×10^{12} particles) yields $(\frac{dP}{df})_{total} \sim 10^{-16}$ W/Hz in the frequency range

from f_c to f_{LHR}. These power spectral densities are much lower than the measured power spectral densities, by about a factor of 10^7 (compare with Figure 6, where $dP/df \sim 10^{-9}$ W/Hz). Therefore, an incoherent process cannot account for the measured wave powers. Some coherent wave process must be involved. In Taylor and Shawhan's [1973] analyses of the generation of VLF hiss emissions by auroral electron beams, the calculated powers for the incoherent Cerenkov process were found to be a factor of 10^2 - 10^3 lower than those measured, again indicating a coherent process.

COHERENT GENERATION MECHANISMS

As concluded in the previous section, some coherent process must be involved in the whistler-mode wave generation from the SL-2 electron beam. Coherent processes can be divided into two classes: direct and indirect. Direct mechanisms involve the direct conversion of energy from an unstable particle distribution to electromagnetic radiation; whereas indirect mechanisms involve the intermediate generation of one or more electrostatic modes which are coupled to the escaping electromagnetic radiation. This section will discuss possible direct and indirect mechanisms that may explain the whistler-mode radiation.

Since an unstable electron distribution is present in the beam the escaping electromagnetic radiation may result from direct conversion of the beam energy to electromagnetic radiation. Such a mechanism has been proposed by Maggs [1976] for the generation of auroral hiss. In his model, incoherent Cerenkov radiation produced by an auroral electron beam is directly amplified via a whistler-mode plasma instability within the beam. It seems reasonable that this wave generation mechanism could be applied to the whistler-mode waves emitted from the SL-2 electron beam; however, a problem arises in doing so. Unlike auroral beams, the path length for wave growth in the SL-2 beam is very short, only two to three electron cyclotron radii (6 to 9 meters). Using the Landau resonance condition and the fact that the emission is

propagating near the resonance cone, we can derive an expression for the wavelength of the whistler-mode radiation,

$$\lambda \cong \frac{V_b}{f} \cos \theta_{Res} \quad , \tag{12}$$

which, for the nominal parameters has a value of about 20 meters. This wavelength is greater than the path length, which completely invalidates any mechanism involving exponential growth. Even if that were not the case, for typical whistler-mode group velocities of 10^7 m/sec, the amount of time the wave spends in the beam is so short, only about 10^{-6} sec, that unreasonably high growth rates ($\gamma > \omega_c \cong 10^6$ sec^{-1}) would be required to generate the radiation. No whistler-mode instability is known that can produce such large growth rates from realistic electron distribution functions. These same conclusions were also reached by Jones and Kellogg [1973] in their paper addressing the growth rates of whistler-mode radiation from artificially-created electron beams.

Next we consider mechanisms involving the intermediate generation of electrostatic waves in the beam. Any density perturbation or bunch created by an electrostatic wave in the beam is capable of emitting coherent Cerenkov radiation. The radiated power from this process will have a frequency spectrum similar to that of a single radiating electron; however, the wave power will be much greater since the emitted power goes as N^2, where N is the number of electrons in a bunch. Coherent Cerenkov radiation from a bunched beam has been considered previously by Bell [1968].

Beam-plasma instabilities are known to be capable of creating intense electrostatic waves and density perturbations in the beam. We estimate the number of coherently bunched electrons required to account for the observed whistler-mode radiation. The total power emitted from the electron bunches in the beam is $(\frac{dP}{df})_{total} = (\frac{dP}{df})_e (\Delta N)^2 \alpha$, where $(\frac{dP}{df})_e$ is the power radiated by each electron, ΔN is the typical number of electrons in a bunch, and α is the number of bunches in the 200 meter segment of the beam. Beam-plasma instabilities are known to create an electrostatic wave near the local electron plasma frequency (3 MHz). Such an emission is, in fact, observed near 3 MHz [see Gurnett et al., 1986]. The corresponding wavelength is $V_b/f_p \simeq 7$ meters, which is assumed to be the approximate length of each bunch. This wavelength can then be used to calculate α, the number of bunches in the first 200 meters of the beam. This number is $\alpha \simeq 29$. Since the radiated power from the 200 meter beam segment, $(\frac{dP}{df})_{total}$, is about 10^{-9} W/Hz, $(\frac{dP}{df})_e$ is about 10^{-29} W/Hz and $\alpha \simeq 29$, each bunch must contain about $\Delta N = 2 \times 10^9$ electrons in order to account for the observed radiated power.

Next we estimate the required electric field strength for the electrostatic wave in the beam that forms the bunches. Assuming that the beam diameter is about 2 cyclotron radii, the electron number density in the bunch can be estimated using the formula:

$$\Delta n = \frac{\Delta N}{\pi r_c^2 \Delta L} \qquad (13)$$

where ΔL is the bunch length and r_c is the cyclotron radius (2 to 3 meters). The required number density is found to be about $\Delta n = 1 \times 10^7$ electrons/m^3. Note that the fractional density perturbation in the beam $\Delta n/n_o$ is only about 0.01; thus, a relatively small perturbation can account for the measured whistler-mode power. Poisson's equation can be used to determine the magnitude of the self-consistent electric field needed to generate this density perturbation

$$\frac{\Delta E}{\Delta L} = \frac{e\Delta n}{\epsilon_o} \quad . \tag{14}$$

From (14), we estimate that an electric field on the order of 1-2 V/m is needed to create the required coherence in the beam electrons.

Although the PDP did not fly directly through the beam during free flight, when the PDP was on the remote manipulator arm, it did provide measurements in the beam. During these times, intense field-aligned electric-field signals near f_{pe} were measured with amplitudes greater than 0.3 V/m, sufficiently large to saturate the receiver. This value is within a factor of 10 of the required amplitudes needed for radiative coherence of the beam electons. The good agreement between the calculated and measured electrostatic field strengths strongly suggests that electron bunches generated by a beam-plasma instability can account for the observed whistler-mode power.

CONCLUSIONS

Like auroral hiss, the whistler-mode radiation from the SL-2 electron beam was found to be progagating near the resonance cone in the same direction as the beam. This conclusion was reached by comparing the measured and modeled electric-field polarizations in the PDP spin plane. The total whistler-mode power radiated by the beam between the shuttle and the PDP was estimated to be 1.6 mW. This represents a conversion of about 3.2×10^{-5} of the beam power to whistler-mode radiation in a path length of 200 meters. The linear emissivity was also observed to decreased with increasing distance along the beam, thereby indicating that most of the whistler-mode radiation is generated relatively close to the source of the beam.

The mechanism that best explains the radiated power and frequency range of the whistler-mode radiation is Cerenkov radiation from coherently radiating electron bunches in the beam. The bunches are most likely created by an electrostatic instability in the beam. The estimated electric field amplitudes required to create the bunching are consistent with the field strength of electrostatic noise measured in the beam.

Future work includes calculating the radiated power from a model electron beam obtained from a particle simulation. The calculated power can then be compared to the measured whistler-mode power to confirm that coherent radiation from electron bunches generate the signal.

ACKNOWLEDGEMENTS

We are grateful to Bill Kurth and John Steinberg for their helpful comments concerning this work. We would also like to thank Terry Averkamp for his valuable input on data analysis and John Birkbeck for a fine drafting job.

Part of this research was funded by NASA Graduate Student Researchers Training Grant NGT-50034. The research at the University of Iowa was also supported by NASA through contract NAS8-32807, grants NGL 16-001-002 and NGL 16-001-043, and by the Office of Naval Research through contract N00014-85-K-0404. The research at Stanford University was supported by NASA through grant NAGW-235.

REFERENCES

Beghin, C., J. P. Lebreton, B. N. Maehlum, J. Troim, P. Ingsoy, J. L. Michau, Phenomena induced by charged particle beams, Science, 225, 188-191, 1984.

Bell, T. F., Artificial production of VLF hiss, J. Geophys. Res., 73, 4409-4415, 1968.

Dechambre, M., Yu. V. Kushnerevsky, J. Lavergnat, R. Pellat, S. A. Pulinets, and V. V. Seleger, Waves observed by the ARAKS experiment: The whistler mode, Ann. Geophys., 36, 351-359, 1980.

Cartwright, D. G., and P. J. Kellogg, Observations of radiation from an electron beam artificially injected into the ionosphere, J. Geophys. Res., 79, 1439, 1974.

Gurnett, D. A., A satellite study of VLF hiss, J. Geophys. Res., 71, 5599, 1966.

Gurnett, D. A., Electromagnetic plasma wave emissions from the auroral field lines, J. Geomag. Geoelectr., 30, 257-272, 1978.

Gurnett, D. A., and L. A. Frank, VLF hiss and related plasma observations in the polar Magnetosphere, J. Geophys. Res., 77, 172, 1972.

Gurnett, D. A., W. S. Kurth, J. T. Steinberg, P. M. Banks, R. I. Bush, and W. J. Raitt, Whistler-mode radiation from the Spacelab-2 electron beam, Geophys. Res. Lett., 13, 225-228, 1986.

Gurnett, D. A., S. D. Shawhan, and R. R. Shaw, Auroral hiss, Z-mode radiation, and auroral kilometric radiation in the polar magnetosphere: DE-1 observations, J. Geophys. Res., 88, 329-340, 1983.

Hartz, T. R., Radio Noise Levels Within and Above the Ionosphere, Proc. ISEE, 57, 1042, 1969.

Inan, U. S., M. Pon, P. M. Banks, P. R. Williamson, W. J. Raitt, and S. D. Shawhan, Modulated beam injection from the space shuttle during magnetic conjunction of STS-3 with the DE-1 satellite, Radio Science, 19, 487, 1984.

James, H. G., VLF observations of auroral beams as sources of a class of emissions, Nature, 224, 351, 1969.

Jones, T. W., and P. J. Kellogg, Plasma waves artificially induced in the ionosphere, J. Geophys. Res., 75, 2166, 1973.

Jorgensen, T. S., Interpretation of auroral hiss measured on OGO-2 and at Byrd Station in terms of incoherent Cerenkov radiation, J. Geophys. Res., 73, 1055, 1968.

Kellogg, P. J., D. G. Cartwright, R. A. Hendrickson, S. J. Monson, and J. R. Winckler, The University of Minnesota electron Echo experiment, Space Res., XVI, 589-599, 1976.

Laaspere, T., and R. A. Hoffman, New results on the correlation between low-energy electrons and auroral hiss, J. Geophys. Res., 81, 524, 1976.

Lin, C. S., J. L. Burch, S. D. Shawhan, and D. A. Gurnett, Correlation of auroral hiss and upward electron beams near the polar cusp, J. Geophys. Res., 89, 925, 1984.

Maggs, J. E., Coherent generation of VLF hiss, J. Geophys. Res., 81, 1707-1724, 1976.

Mansfield, V. N., Radiation from a charged particle spiraling in a cold magnetoplasma, Astrophy. J., 147, 672, 1967.

Monson, S. J., P. J. Kellogg, and D. G. Cartwright, Whistler-mode plasma waves observed on electron Echo II, J. Geophys. Res., 81, 2193, 1987.

Mosier, S. R., and D. A. Gurnett, VLF measurements of the Poynting flux along the geomagnetic field with Injun 5 satellite, J. Geophys. Res., 74, 5675-5687, 1969.

Mosier, S. R., and D. A. Gurnett, Theory of the Injun 5 very-low-frequency Poynting flux measurements, J. Geophys. Res., 76, 972-977, 1971.

Shawhan, S. D., G. B. Murphy, P. M. Banks, P. R. Williamson, and W. J. Raitt, Wave emissions from D. C. and modulated electron beams on STS-3, Radio Science, 19, No. 2, 471-486, 1984.

Smith, R. L., VLF observations of auroral beams as sources of a class of emissions, Nature, 224, 351, 1969.

Stix, T. H., The Theory of Plasma Waves, McGraw-Hill, New York, 1962.

Taylor, W. W. L., and S. D. Shawhan, A test of incoherent Cerenkov radiation for VLF hiss and other magnetospheric emissions, J. Geophys. Res., 79, 105-117, 1974.

Winckler, J. R., The application of artificial electron beams to magnetospheric research, Rev. Geophys. Res. and Space Phys., 18, No. 3, 659-682, 1980.

FIGURE CAPTIONS

Figure 1 A frequency vs. time spectogram from the PDP plasma wave instrument showing intense emissions during a D.C. electron gun firing. The funnel-shaped structure that extends from the electron cyclotron frequency, f_c, to about 30 MHz is whistler-mode radiation from the beam.

Figure 2 This diagram shows the index of refraction surface for the whistler mode and the associated $\overline{E}$, $\overline{k}$, and $\overline{v}_g$ vectors for propagation near the resonance cone ($\theta \simeq \theta_{Res}$). For propagation near the resonance cone, $\overline{k}$ and $\overline{E}$ are parallel and nearly perpendicular to $\overline{v}_g$. In this limit $\overline{E}$ is linearly polarized and quasi-electrostatic.

Figure 3 This figure shows the whistler-mode ray paths from a point source radiator. Note that a passing spacecraft will detect radiation near the gyrofrequency, first, then detect lower frequency emissions as it nears the source. A well-defined frequency versus time funnel-shaped spectra results from this spacecraft/source encounter.

Figure 4 This diagram shows the ray path and $\overline{E}$, $\overline{k}$, and $\overline{v}_g$ vectors used to confirm the electric field polarization. The assumed electric field is projected into the PDP spin

plane and the angle relative to the projection of the sun vector is calculated. The projected electric field direction can then be compared to the measured directions calculated from spin modulation maximums in the electric field intensity (see Figure 4).

Figure 5(a), (b), (c), and (d) These plots show the relative directions of the computed and measured electric-field vectors in the PDP spin plane for the 562 kHz, 311 kHz, 178 kHz, and 100 kHz frequency channels. The dots represent the computed electric field directions assuming that the wave vector is near the resonance cone with $\overline{k} \cdot \overline{v}_b > 0$, and the x's represent measured electric-field directions. The close agreement between the measured and modeled directions indicates that the whistler-mode radiation is propagating near the resonance cone in the same direction as the beam.

Figure 6 This diagram shows the integration surface used to calculate the power emitted from the beam in the whistler mode. At closest approach, the PDP passed within 3 meters of the beam at a distance of about 200 meters from the shuttle.

Figure 7 The calculated power spectral density from the beam in the whistler mode is shown as a function of frequency.

Figure 8(a) and (b) The linear emissivity, $dP/df d\ell$, is shown as a function of the distance, L, along the beam for the 562 kHz and 311 kHz frequency channels. Note that the

emissivity starts to decrease rapidly beyond about 100 meters.

Figure 9 The power spectra from a single electron radiating via the Cerenkov processes is shown in a plasma environment similar to that surrounding the SL-2 beam. These calculations assume the wave/beam interaction is by a Landau resonance process and that the particle pitch angle is 10°. This power calculation is based on formulas derived by Mansfield [1967].

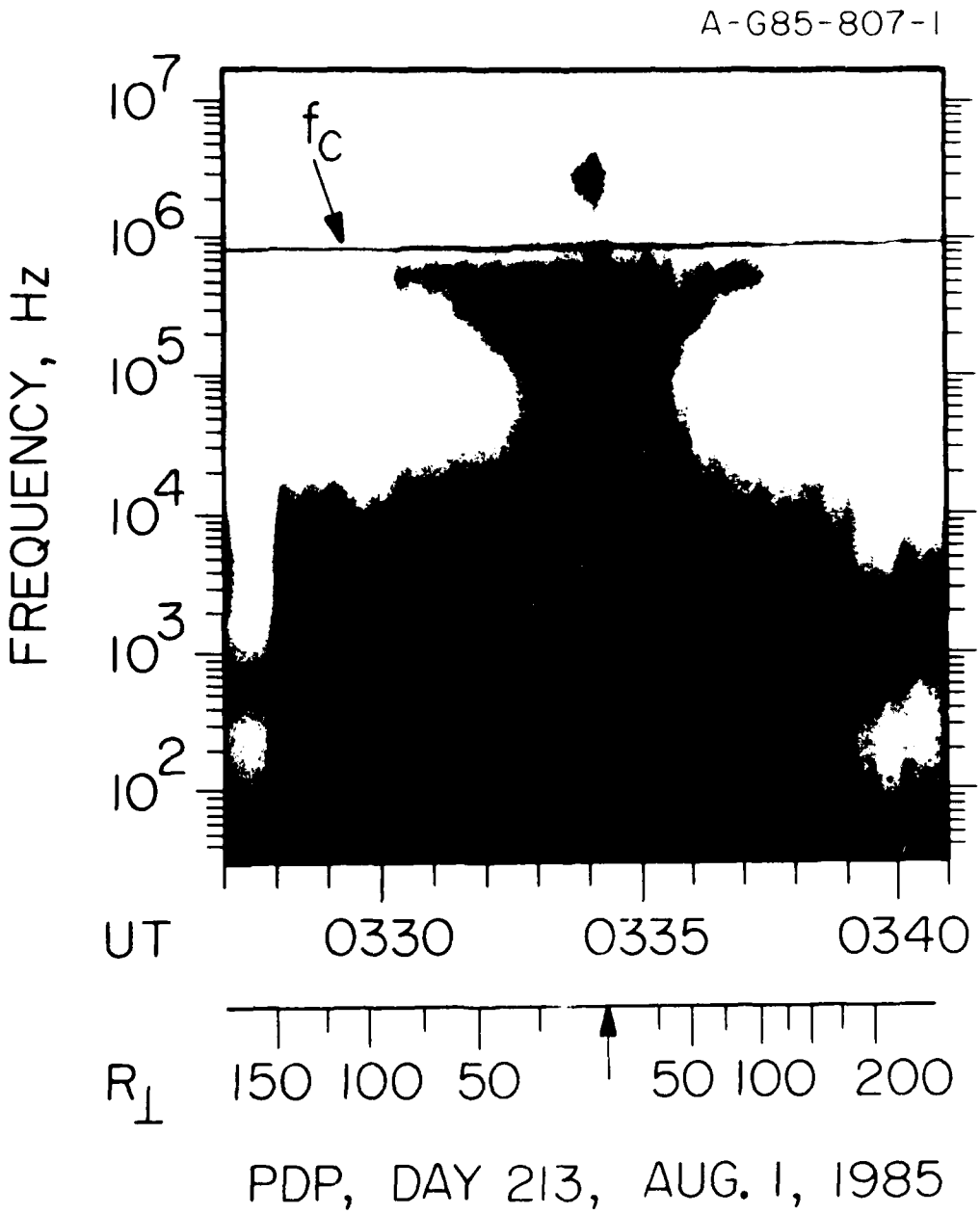
A-G85-807-1
FREQUENCY, Hz
10^7
10^6
10^5
10^4
10^3
10^2
f_c
UT
0330
0335
0340
$R_\perp$
150 100 50
50 100 200
PDP, DAY 213, AUG. 1, 1985

Figure 1

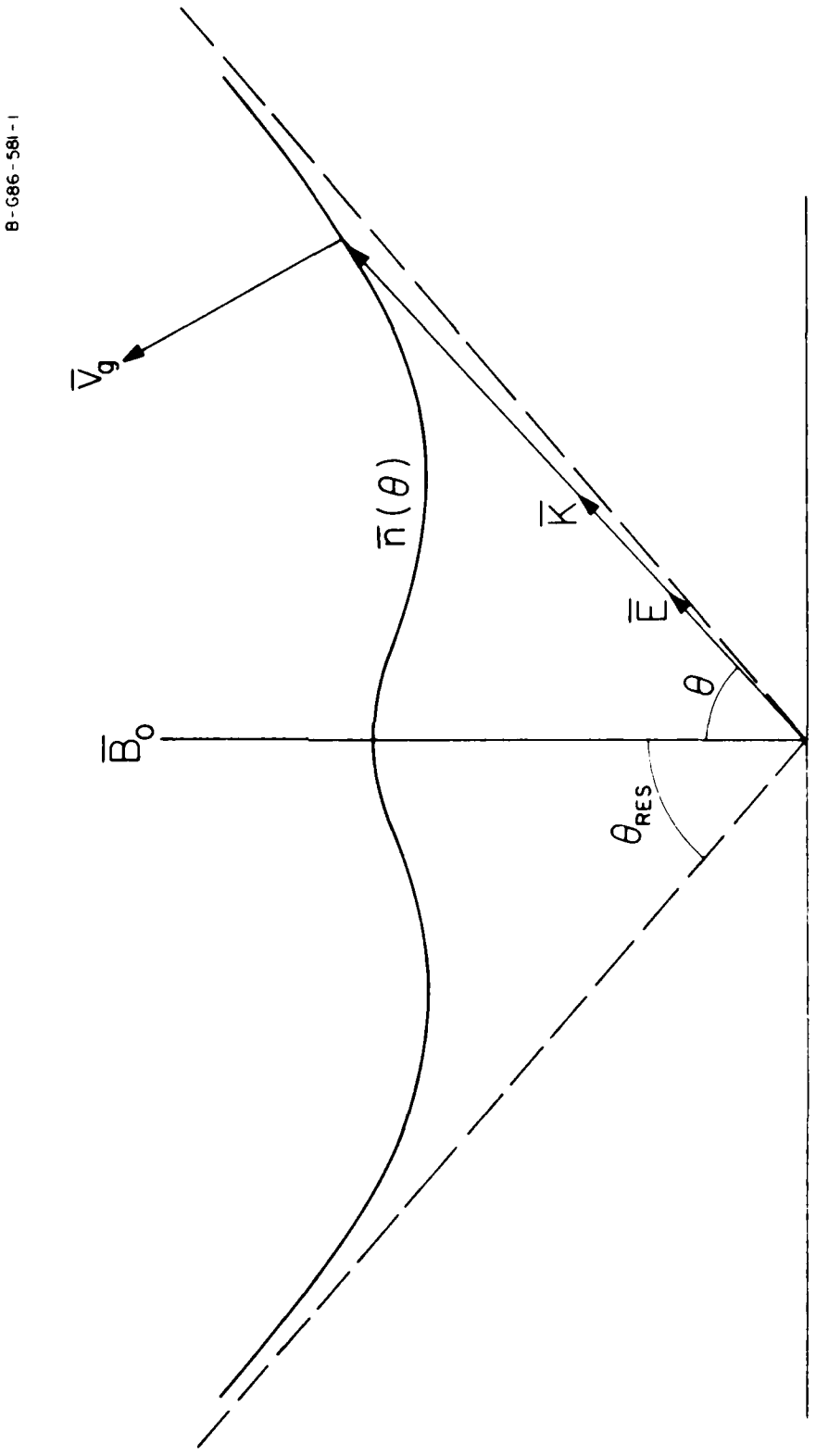

Figure 2

B-G85-792

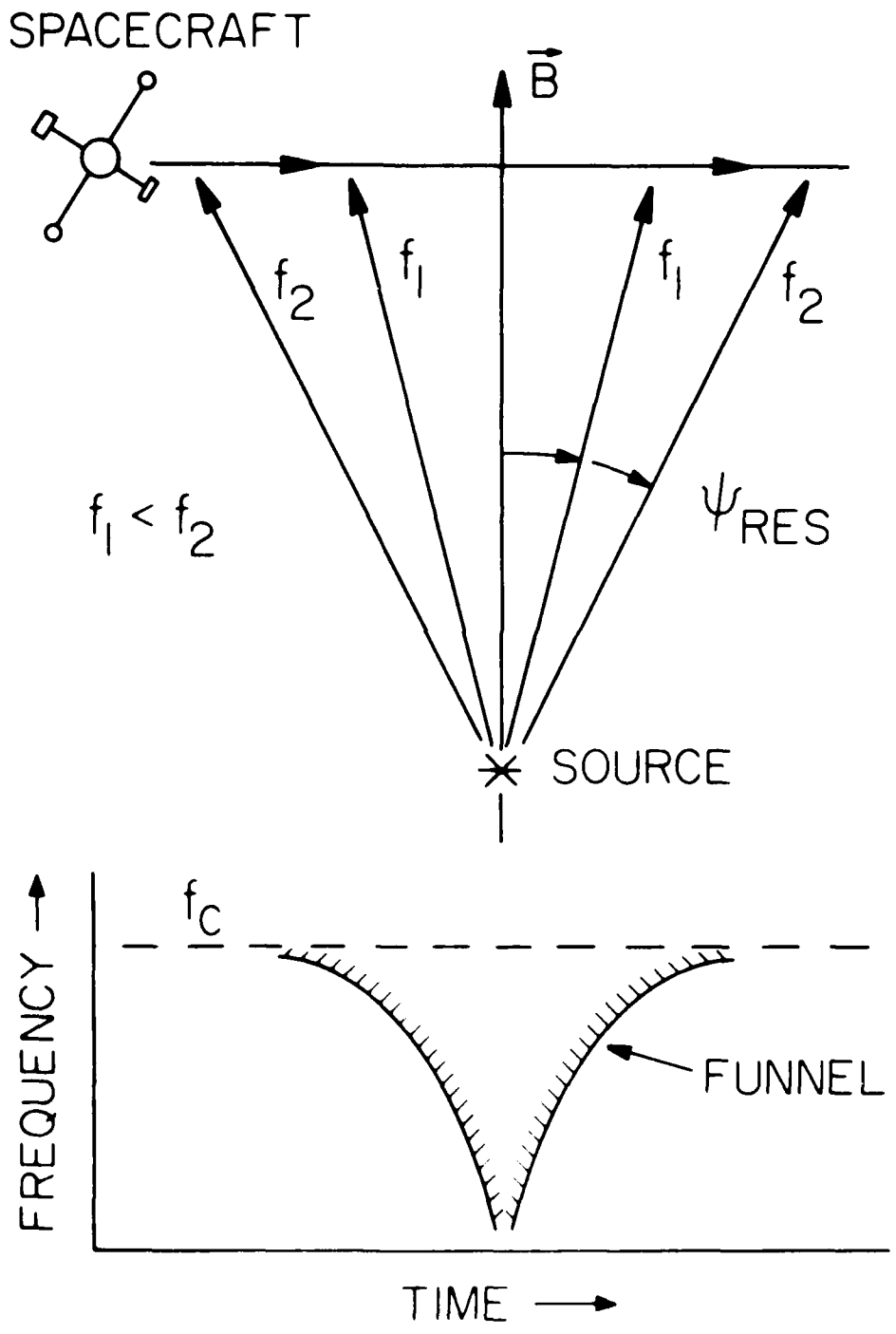

Figure 3

B-G86-582-1

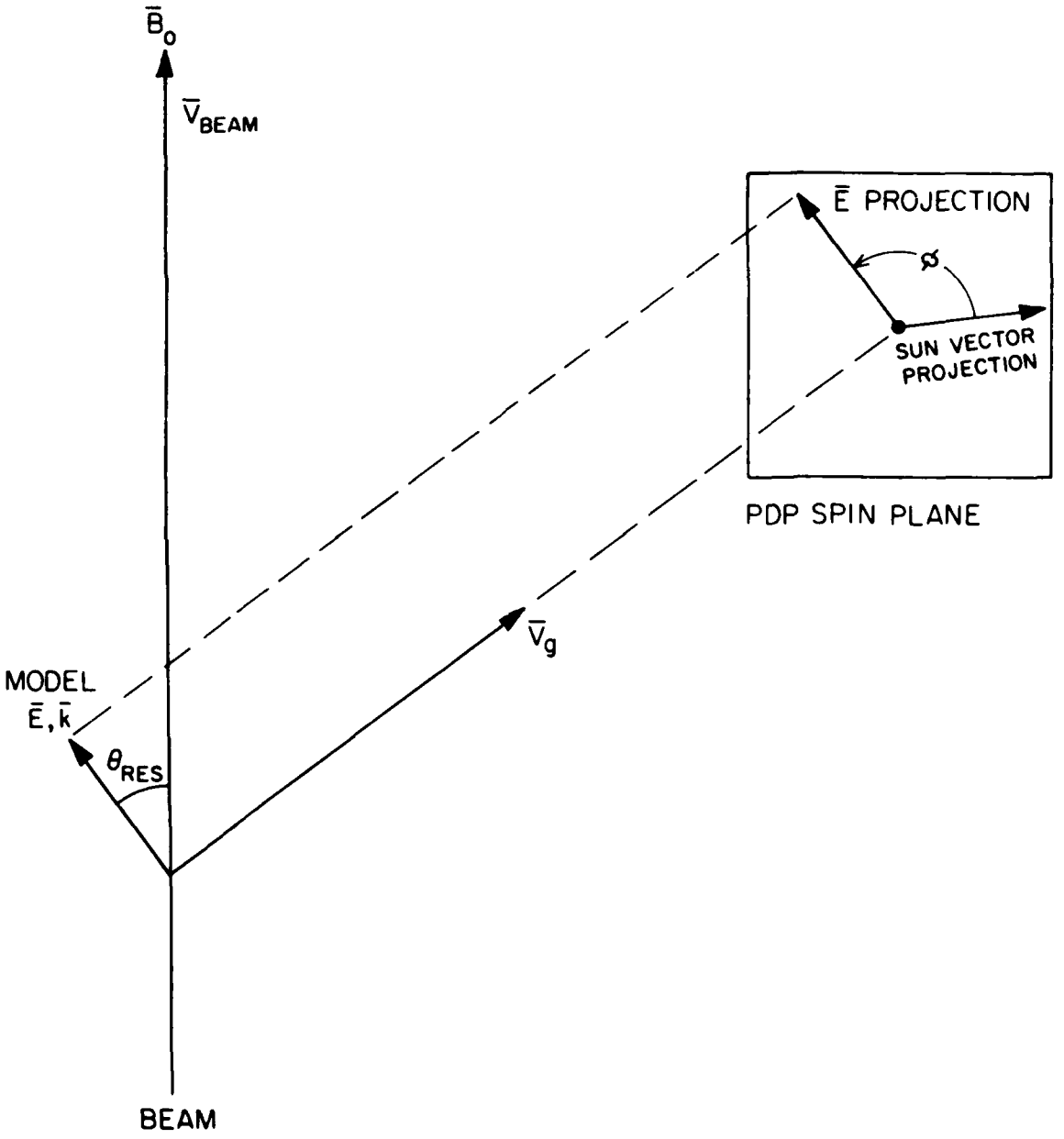

Figure 4

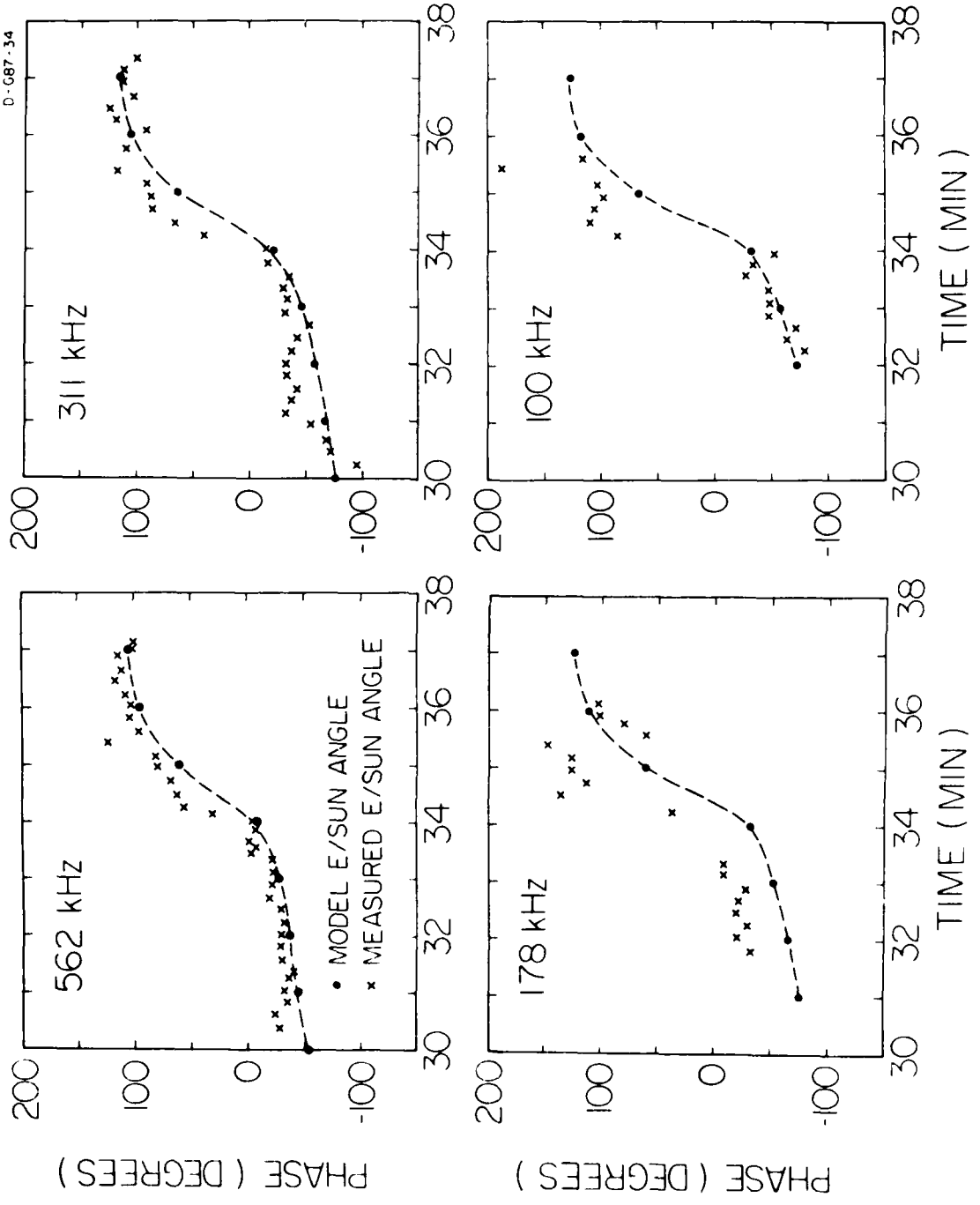
D-687-34
562 kHz
311 kHz
178 kHz
100 kHz
• MODEL E/SUN ANGLE
× MEASURED E/SUN ANGLE
PHASE (DEGREES)
TIME (MIN)
200
100
0
-100
30
32
34
36
38

Figure 5

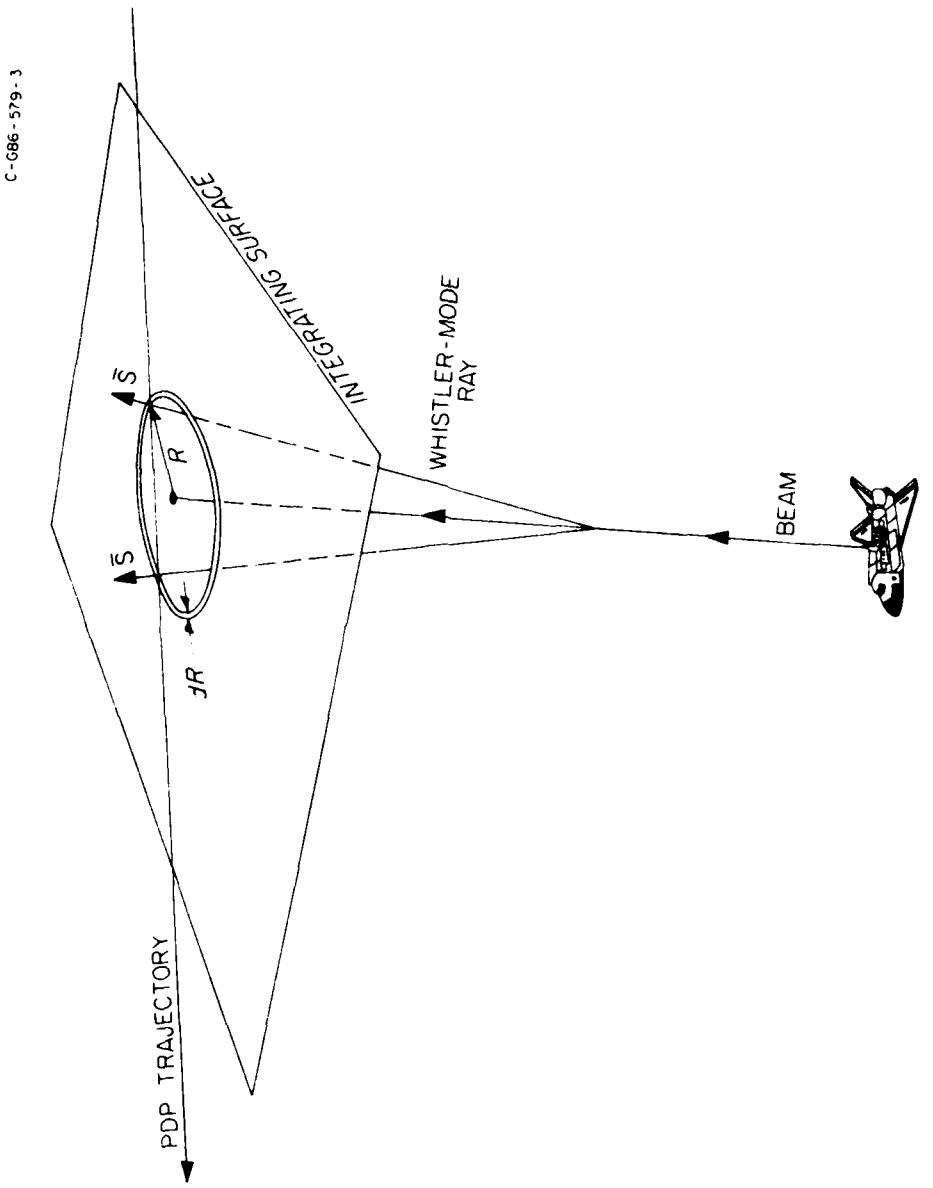
C-086-579-3
INTEGRATING SURFACE
WHISTLER-MODE RAY
BEAM
PDP TRAJECTORY
R
δR

Figure 6

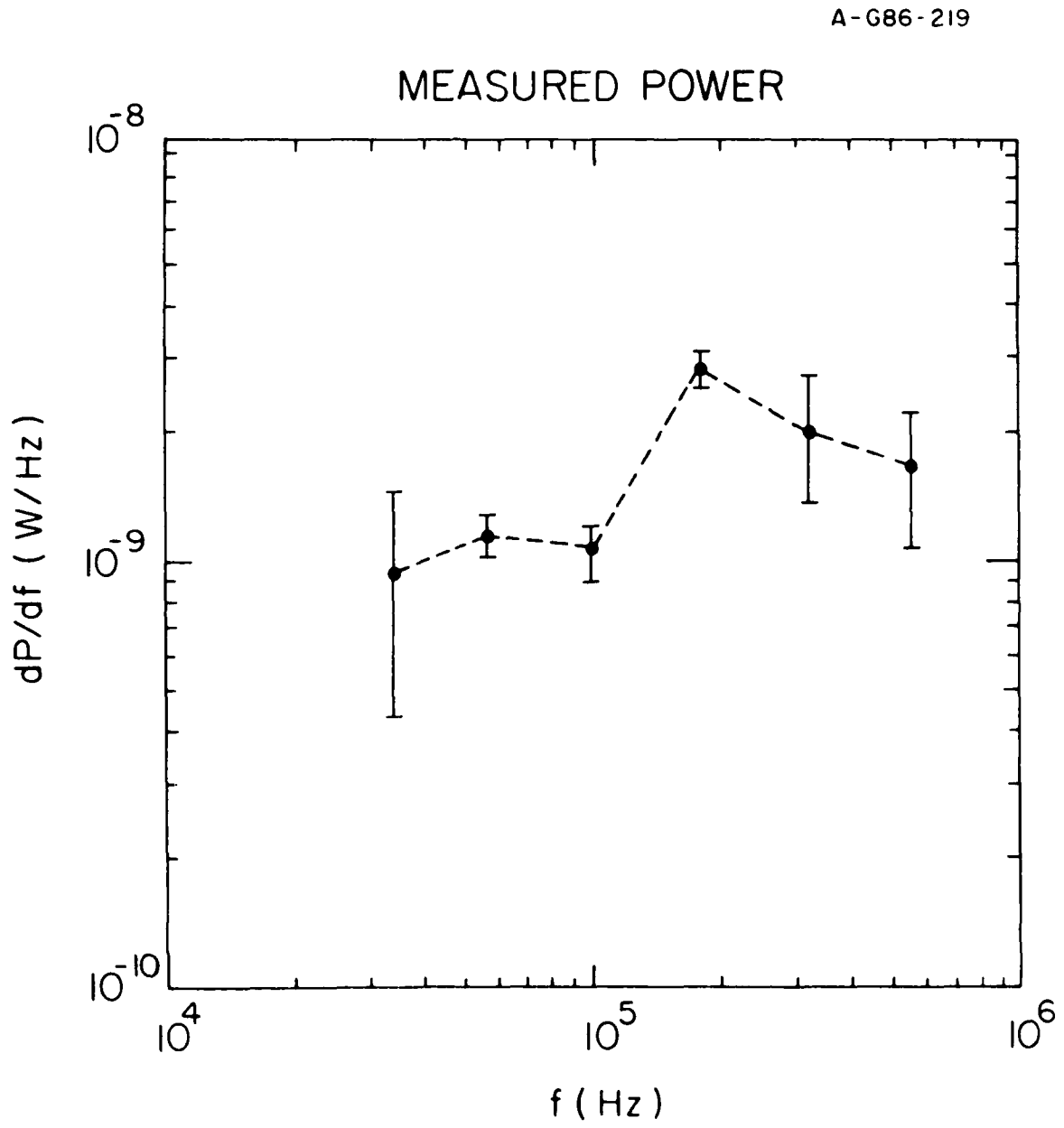

Figure 7

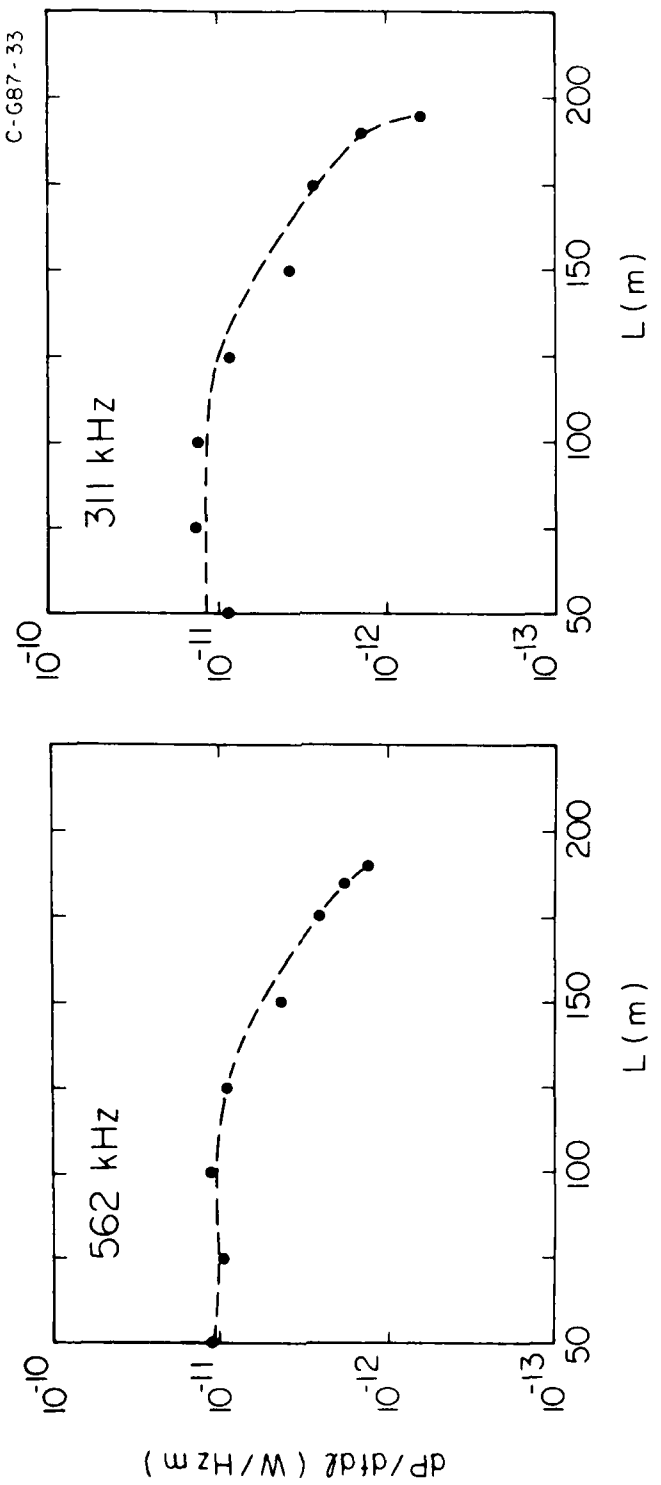
C-G87-33
311 kHz
562 kHz
dP/dfdℓ (W/Hz m)
L (m)
10^-10
10^-11
10^-12
10^-13
50
100
150
200

Figure 8

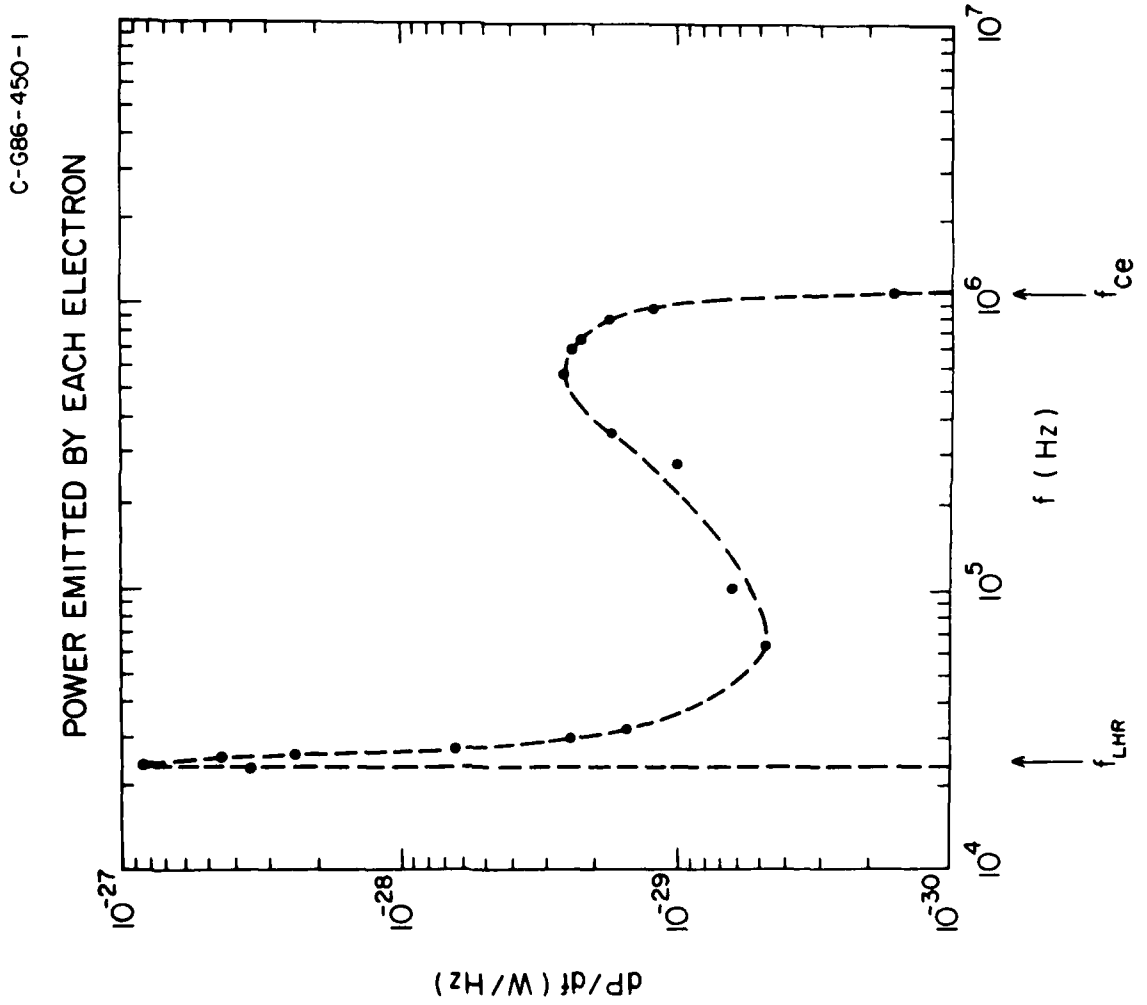
C-G86-450-1
POWER EMITTED BY EACH ELECTRON
dP/df (W/Hz)
10^-27
10^-28
10^-29
10^-30
10^4
10^5
10^6
10^7
f (Hz)
f_LHR
f_ce

Figure 9

END

FILMED

MARCH, 1988

DTIC